(This is a sample cover image for this issue. The actual cover is not yet available at this time.)

Journal of Neuroscience Methods 205 (2012) 159–168

Contents lists available at SciVerse ScienceDirect

Journal of Neuroscience Methods

journal homepage: www.elsevier.com/locate/jneumeth

Basic Neuroscience

An *in vitro* injury model for SH-SY5Y neuroblastoma cells: Effect of strain and strain rate

Maciej Skotak, Fang Wang, Namas Chandra *

Department of Mechanical and Materials Engineering, University of Nebraska-Lincoln, Lincoln, NE 68588-0526, USA

ARTICLE INFO

Article history:
Received 29 September 2011
Received in revised form
29 December 2011
Accepted 5 January 2012

Keywords:
In vitro TBI model
Strain and strain rate effect
Viability scale
Stretch induced injury

ABSTRACT

There is a great need to have *in vitro* cell injury model wherein a wide range of strain (ε) and strain rate ($\dot{\varepsilon}$) can be precisely and independently applied. Such a model will enable exploration of various biomechanical loading conditions cells normally encounter during either blunt or blast impact-induced traumatic brain injuries (TBIs). In combination with a highly automated data acquisition and analysis system, this method can quickly generate a large data set of experimental results to yield identification of bio-mechanical and chemical sequelae following injury. A proper understanding of these sequelae will enable the discovery of the time window of opportunity available for pharmacological interventions. In this study we present such an injury model, a modified version of the Cultured Axonal Injury (CAI) device, and demonstrate its efficacy through viability of SH-SY5Y cells at different ranges of strain (0–140%) and strain rate (15–68 s^{-1}). We identified three different regimes in the stretch-induced dose–response of curves of SH-SY5Y cells, with a very sharp decline from live to dead in a narrow range of strain (30–55%). The effect of strain rate is minimal when the final strain in the cells was fixed at 50%. The model further shows that time-after-injury plays a vital role in the determination of recovery-deterioration pathways and the biological selection depends on the severity of initial injury. These data point out the initial strain level is vital to the cell fate and emphasize the need to study the various mechanisms triggered by different magnitudes of initial injuries.

1. Introduction

The Centers for Disease Control and Prevention estimates that approximately 1.4 million US individuals sustain traumatic brain injuries (TBIs) per year (Nampiaparampil, 2008). TBIs are caused by ballistic, blunt and blast impacts triggering different biomechanical loading conditions leading to different types of injuries. *In vitro* model hinges on the hypothesis that though there are multiple loading conditions at the body or organ level, there are limited states of biomechanical loadings at the cellular levels (LaPlaca and Prado, 2010; Morrison et al., 1998b). *In vitro* traumatic brain injury (TBI) cellular models are developed with intent to understand the effects of the biomechanical loading conditions at the cellular level (Chen et al., 2009; Morrison et al., 1998b, 2011). The primary goal of an injury model will be to accurately apply specified biomechanical loading conditions to a tissue (in 2D or 3D form, or cells) and delineate the mechanical and biochemical pathways post-injury, both in the acute and chronic phases. The ultimate objective is to seek therapeutic interventions to judiciously alter the pathway resulting in the mitigation or elimination of the detrimental effects of TBI.

During a traumatic event, cells experience mechanical insult, which at the *in vitro* loading level can be assigned into one of the elementary modes of injury: stretching, compression, torsion or shear or a combination thereof. The stretch model is widely studied due to its elemental nature of loading; all such stretch injury models comprise an elastic membrane with a layer of dissociated adherent cells (the so-called 2D system). Ellis et al. (1995) were one of the very first to use the *in vitro* stretch model which was applied to evaluate injury of astrocytes. Positive pressure pulse was used in their apparatus to control the level of deformation of the silastic membrane and corresponding degree of injury. The maximum strain levels (Table 1) were characterized using three methods, but at that time technology allowing precise real-time membrane deformation tracking was not available. Ellis and co-workers devised the arbitrary injury scale based on strain levels applied to cells: 31% – mild, 38% – moderate and 51% – severe. This stretch injury model was used extensively by Webber group (Engel et al., 2005; Slemmer et al., 2002, 2004) in the research of cell cultures composed of cortical, hippocampal and cerebellar neurons and glia. Cultured Axonal Injury (CAI) device, operating, in essence using the same principle as Ellis' model, was developed at the University of Pennsylvania in the late 1990s (Smith et al., 1999) for the sole purpose of applying uniaxial stretch to investigate axonal injury. This model was further expanded by modification, which allowed uniaxial and biaxial

* Corresponding author.
E-mail address: nchandra2@unl.edu (N. Chandra).

0165-0270/$ – see front matter © 2012 Elsevier B.V. All rights reserved.
doi:10.1016/j.jneumeth.2012.01.001

Table 1
Contemporary stretch injury models.

Injury model	Cell type	Reported		Reference
		Strain, %	Strain rate, s^{-1}	
Uniaxial strain				
PP	N-Tera2 differentiated	58–77	26–35	Smith et al. (1999)
VCA	NG108-15 differentiated	20–70[a]	20–90[a]	Pfister et al. (2003)
Biaxial strain				
PP	Astrocytes	<72	1.5–6[b]	Ellis et al. (1995)
PP	Neurons on glia-support	0–50[c]	–	Geddes-Klein et al. (2006)
	Neurons/neuron-glia	0–50	–	Lusardi et al. (2004a)
NP	NG108-15 differentiated	7–45	<1, 10	Cargill and Thibault (1996)
NP	–	0–65	15	Morrison et al. (1998a)
	Organotypic	0–47	0–22	Morrison et al. (2000)
Equibiaxial strain				
I	Organotypic[d]	0, 10, 35[e]	10, 20[e]	Morrison et al. (2006)
I	Organotypic[d]	0–50[e]	0–50[e]	Cater et al. (2006)
I	Organotypic[f]	0–50	0–35	Elkin and Morrison (2007)

I – indenter, NP – negative pressure, PP – positive pressure, VCA – voice coil actuator.
[a] Mechanical capabilities of the device listed, only preliminary results reported.
[b] Maximum achievable strain rate: 20 s^{-1} (Morrison et al., 2006).
[c] Membrane rupture prevented validation of strains higher than 50%.
[d] Hippocampal slice culture.
[e] Mechanical capabilities of the injury device claimed by authors: $5\% < \varepsilon < 100\%$, $0.1 < \dot{\varepsilon} < 150\ s^{-1}$.
[f] Cortical slice culture.

stretching of neurons (Geddes-Klein et al., 2006). In both models, there was an immediate increase of intracellular free calcium concentration ($[Ca^{2+}]_i$) which was an order of magnitude higher for biaxially stretched neurons.

Though there are many cell injury models (see Table 1), in general, most of them suffer in their inability to achieve a non-uniform strain field (Morrison et al., 2011). Furthermore, in many cases though the strain levels are measured on the substrate, that does not guarantee that the cells also experience the same stretching. The non-uniformity of the strain-field can be mitigated through data analysis on the center area of the specimen (Geddes-Klein et al., 2006). To address non-uniformity in the stress field advanced 2D *in vitro* TBI models were developed. The injury model of Morrison et al. (2006) uses planar elastic membrane deformation and allows precise control over biaxial strain field (5–100%) and testing of TBI pertinent strain rates up to 50 s^{-1}. With this model organotypic culture were tested using 0–50% strain and 0–50 s^{-1} strain rate ranges (Cater et al., 2006; Elkin and Morrison, 2007). Most popular contemporary stretch injury models are summarized in Table 1. We have addressed the issues of cell vis-à-vis the substrate deformation in this work, through additional analysis. However, substrate strain is used in this paper as a characteristic parameter, due to complications in validation of the true strain experienced by cells.

High throughput *in vitro* models can utilize human cell lines and study the impact of mechanical injury to these cells. SH-SY5Y is a human neuroblastoma cell line, which has been applied in many neurological experiments such as Parkinson's disease (PD) (Decressac et al., 2011), Alzheimer's disease (AD) (Bose et al., 2011) and traumatic brain injury (TBI) (Arun et al., 2011). Though SH-SY5Y cells do not fully follow the biochemical sequelae post-injury, many of the characteristics are representatives of certain important class of neurological disorders. For example, in the case of PD, these cells express tyrosine hydroxylase and dopamine-β-hydroxylase, as well as the dopamine transporter; similarly in the case of AD, SH-SY5Y cells can release amyloid-β (Aβ) treated by stress related MAPKs activator. In both the cases, the mechanisms of oxidative damage and mitochondrial dysfunction are fully represented in these cell lines.

The purpose of this study is to develop an *in vitro* model to produce a wide range of strain and strain rates to determine the effect of these cell-stretching in TBI. In this study, we modified the CAI device to control the magnitude of deformation and through these modifications achieved the wide range of strain and strain rate. We then precisely calibrated different levels of strain and strain rate using advanced high-speed imaging system. By combining Live–Dead assay with Laser Scanning Cytomertry (LSC), a high throughput spectroscopic analysis was introduced to evaluate the efficacy of this model in SH-SY5Y cells. Based on these data, stretch-injury tolerance levels for SH-SY5Y cells with an aid of dose–response model and temporal injury evaluation can be very easily established.

2. Materials and methods

2.1. Cell culture

Human neuroblastoma SH-SH5Y cells were obtained from American Tissue Culture Collection (ATCC) and cultured in Dulbecco's modified Eagle's medium (DMEM, GIBCO) supplemented with 10% heat-inactivated fetal bovine serum (GIBCO), 100 U/mL penicillin, 100 μg/mL streptomycin (GIBCO) and 2 mM L-glutamine. Cells were grown in the Heracell 150i CO_2 incubator at 37 °C and 100% humidity atmosphere (5% CO_2 and 95% air, sterilized using 0.2 μm filter). For all experiments, cells were plated at a density of $10^4/cm^2$ on flexible, transparent silicone substrates (Gloss/Gloss, 0.005″ thick, Specialty Manufacturing Inc., Saginaw, MI, USA) that were previously coated overnight with 100 μg/mL poly-L-lysine hydrobromide (PLLY, molecular weight M_w = 150,000–300,000 Da, Sigma) at room temperature. Typically, cells were kept below 20 passages in all experiments.

2.2. Mechanical testing

The CAI device was originally designed to study axonal injury and was modified to achieve high strain and strain rates for the whole neuronal body (including soma, dentrites and axons), independently study strain rate effects and extend strain rate range. We altered the configuration with:

1. a circular opening (20 mm OD) in the bottom plate (Geddes-Klein et al., 2006),
2. an acrylic fixture (Fig. 1), which allows strain rate evaluation at ε = 50%,

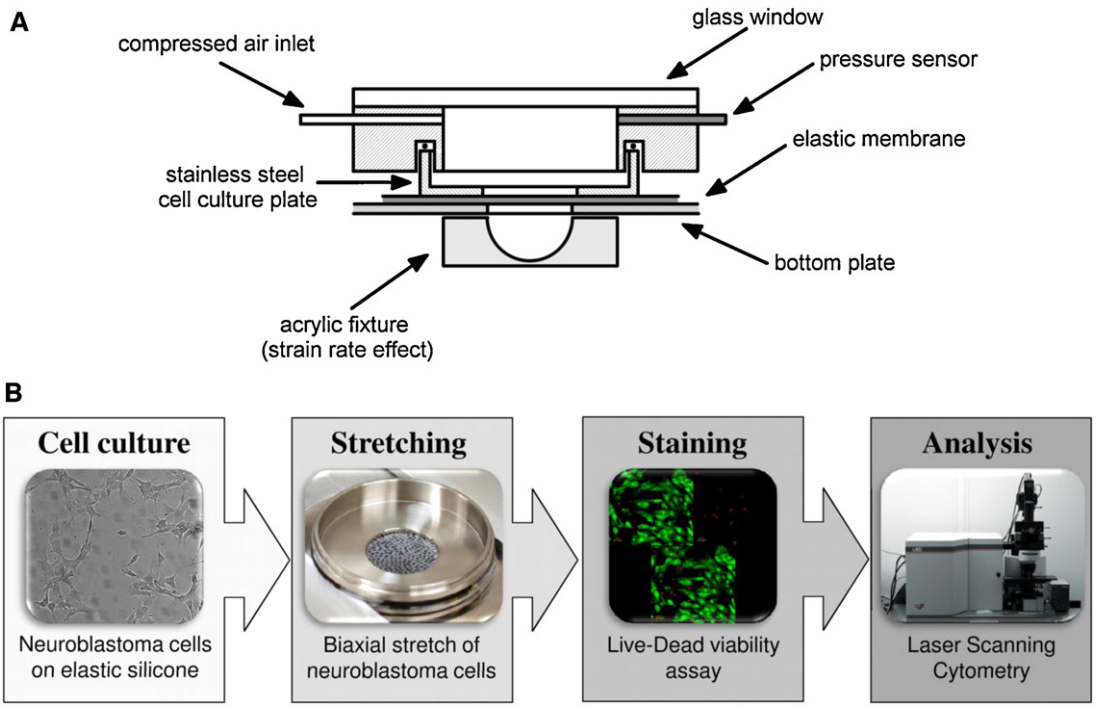

Fig. 1. (A) Schematic representation of the stretch injury device. Elastic membrane is attached to the stainless steel cell culture dish and the cells are grown in the central circular opening. The membrane with cells is deformed by impulsive pressurization. The removable fixture made of acrylic glass at the bottom is used to restrict the deformation of the membrane. By controlling the speed of the deformation, the strain rate effects are investigated. (B) The workflow chart of the *in vitro* TBI model.

3. a toroidal silicone inserted to control internal volume of sample chamber and achieve higher strain rates.

When the substrate is stretched, a small central region is stretched biaxially; therefore, all tests described herein are subject to biaxial stretching. The mechanical tests were performed on the third day after seeding the cells using the device depicted in Fig. 1. Evaluation of acute cellular response took place after the media were aspirated, and cells were washed with three 2 mL aliquots of sterile Dulbecco's PBS (D-PBS). Then 1 mL of sterile D-PBS was added to the cell culture, the dish was enclosed and the air pulse with predefined nominal setting was applied. Nominal settings (inlet pressure, pulse duration time) with corresponding values of maximum strain calculated using Eq. (1), are listed in Table 2. Additionally, in the last column average values of strain rates corresponding to nominal pressure are specified. The dish was then immediately removed, and cells were stained with Live–Dead assay. For time dependent studies, essentially the same procedure was repeated with two modifications: (1) the stretching tests were conducted in DMEM, (2) the cell culture dish was transferred to the incubator and kept there for the predefined amount of time.

2.3. Calibration of strain and strain rate

The strain mapping was performed using ARAMIS system (GOM, Braunschweig, Germany). Two methods of calibration were used (Figs. 2 and 3). First, the system with two FASTCAM SA1.1 high-speed cameras (Photron, San Diego) was used, which allows full 3D strain calibration (Fig. 2A). In these experiments, the area of interest of the matt silicone (M/M) was painted with flat white paint, and the stochastic pattern was applied manually with a Sharpie pen. Then, the membrane was mounted on a stainless steel culture dish and placed in the CAI device, with painted surface on the outside. The device was facing the cameras and illuminated with MI-150 fiber optic illuminator (Edmund Optics, Barrington, NJ). The pressurized air pulses with predefined nominal settings of pressure and time (Table 2) were then applied, and the PDMS membrane deformation history was captured with resolution of 512×512 pixels at 5000 frames per second. All calibration runs were repeated at least three times. Second calibration method, was used to verify the results from 3D calibration (Fig. 3) and calculate the strain magnitude (ε_{max}) for the gloss (G/G) PDMS membrane used in experiments with cells. The CAI device was positioned perpendicularly to the camera, and only one high speed camera was used to capture the displacement of the G/G PDMS membrane. Image analysis yielded values of maximum displacement ($d_{G/G}$, Fig. 3B) for every set of nominal conditions, and these were later on used to calculate the strain values.

Fast image acquisition speeds (5000 fps, corresponding to 0.2 ms per frame) allowed us to precisely calculate strain rates for every calibration run. The time at the "zero" strain value immediately before the onset of membrane deformation was subtracted from the time at the strain peak (Fig. 2B) and this value was used to calculate the strain rate, *i.e.* $\dot{\varepsilon} = \varepsilon_{max}/\Delta t$. The measurements of strain rate effect were conducted using a fixture made of acrylic glass, which had a machined concave hemisphere with 10 mm radius and 10 mm depth (Fig. 1A). The geometry of the concave hemisphere corresponds to the strain value $\varepsilon = 50\%$ according to the 3D calibration data. The fixture was attached at the bottom of the CAI device to limit the deformation of the silicone membrane.

2.4. Live–Dead assay

Viability and membrane permeability (injury levels) of cells subjected to different levels of strain and strain rates (Table 2) was evaluated *via* Live–Dead assay (Invitrogen, Carlsbad, CA). All tests were repeated in quadruplicates, unless indicated otherwise. The cells were stained with 2 μM calcein-AM and 4 μM ethidium homodimer-1 (EthD-1) for 30 min at 37 °C immediately after injury or at predefined time points (typically 1, 2, 4, 12 and 24 h) to evaluate the recovery, followed by fixation with 4% formaldehyde solution in D-PBS. The silicone membrane with the stained cells

Table 2
Nominal settings (pressure and time) used in this study with corresponding maximum substrate strain (%) and average strain rates.

Nominal pressure, psi	Nominal time, ms[a]							Strain rate, s^{-1}
	7	10	15	20	25	30	50	
5		10	25	35	42	52[b]	74	15
10		23	50	67[b]	80	88		25
15	22	41[b,c]	73[b]	90				33
20	34	61[b,c]	89	121				42
25	45	75	110	140				50

[a]The nominal time is the pulse duration time, and a measured time to peak deformation is used to calculate the strain rate.
[b]Nominal settings used in the strain rate evaluation experiment (Fig. 6).
[c]Silicone circular insert was placed in the sample chamber to decrease internal chamber volume. This in turn helped increase the strain rate to 61 and 68 s^{-1} for 15 psi–10 ms and 20 psi–10 ms, respectively.

was subsequently washed three times with D-PBS and mounted on the glass slide. Samples were stored in the darkness at 4 °C before analysis.

2.5. Laser Scanning Cytometry

Briefly, Laser Scanning Cytometer (CompuCyte, Westwood, MA) equipped with 405 nm UV, 488 nm Argon and 633 nm HeNe lasers and motorized stage was used to scan the circular area of the sample (20 mm OD) using 20× magnification objective. Signals from labeled cells were detected with photomultiplier tube (PMT) detectors using 530/30 nm (green) and 650/LP (red) filters, respectively. The sensitivity of the detectors was kept constant during all measurements. The contouring of the cells was performed over the sum of green and red channels to take into account all cells with different viability levels. Then, integrals of analytical signals were used to construct the ratiometric viability scale based on the measurements of control samples with live and dead cells only. These

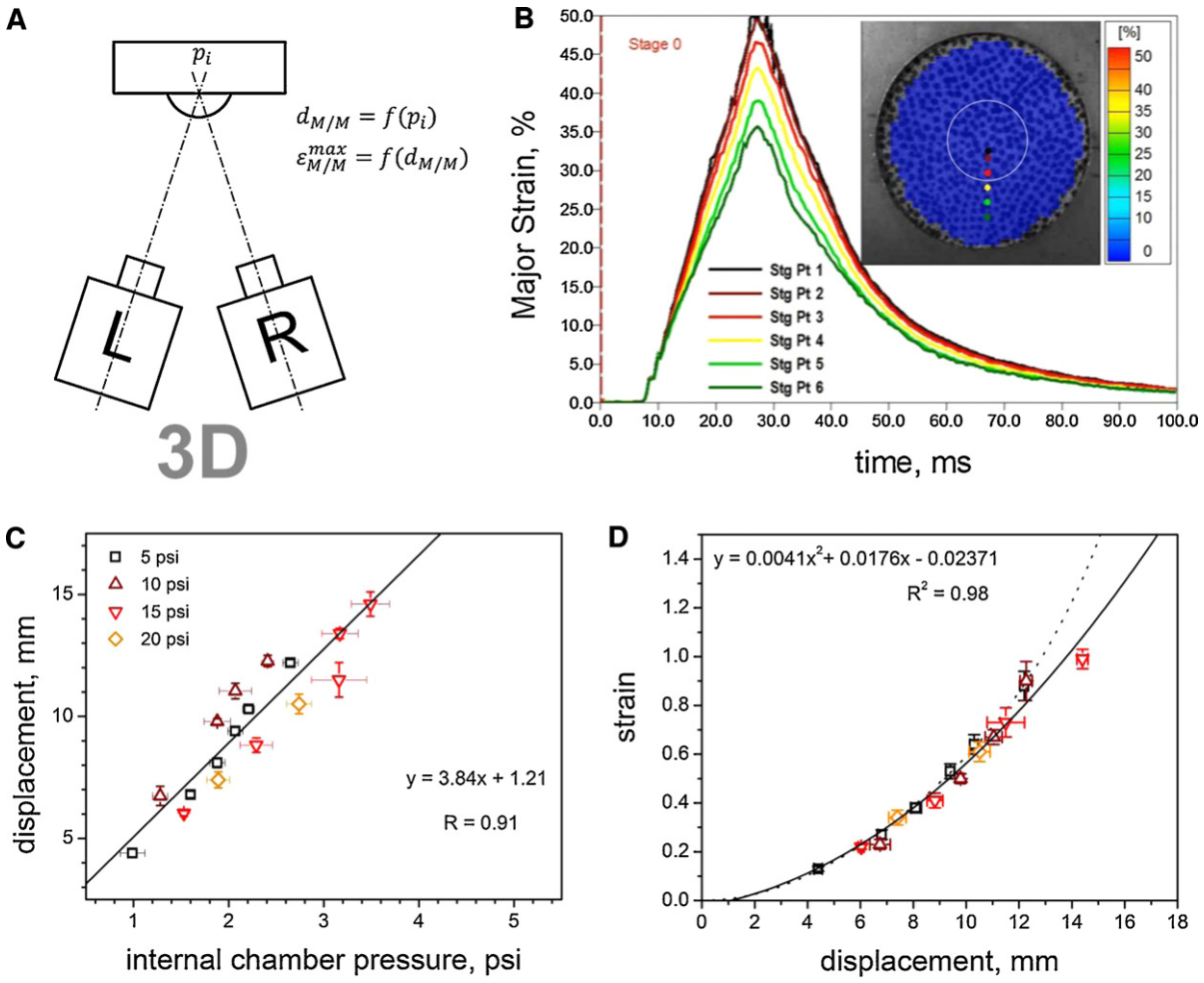

Fig. 2. (A) Schematic representation of strain mapping measurements in 3D configuration The L and R letters represent high speed cameras used in these experiments. (B) The strain history of the PDMS membrane subjected to 10 psi–15 ms pulse (nominal time and pressure values are listed in Table 2). The images were recorded using the high-speed ARAMIS 3D system at 5000 fps. The strain *versus* time plots at six different locations is presented. All respective points are indicated in the inset as color dots. (The inset shows the PDMS membrane with applied stochastic pattern and overlaid calculated strain map (blue color) at time t_o = 0 ms (stage 0).) (C) The displacement (d) as a function of the internal chamber pressure (p_i) calibration curve for opaque (M/M) silicone. (D) Maximum strain-displacement relationship ($\varepsilon^{max} = f(d)$) predicted by theory (Eq. (1), dotted line) and experimental data fitted using presented equation (solid line). (For interpretation of the references to color in this figure legend, the reader is referred to the web version of the article.)

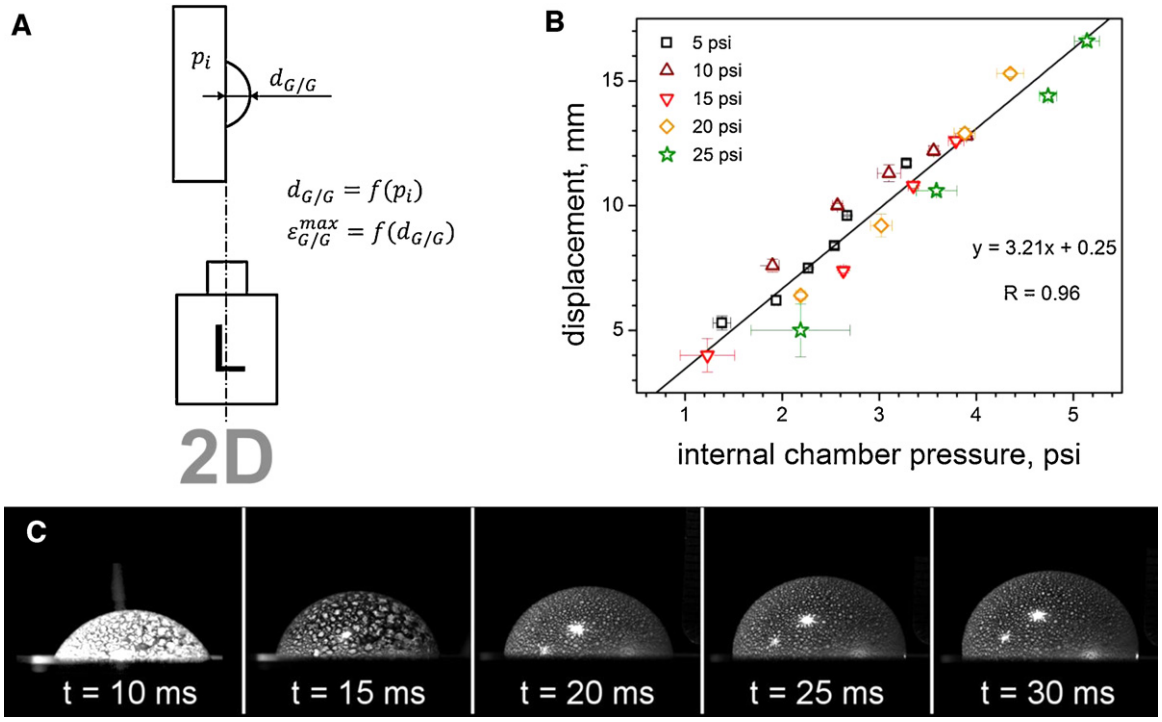

Fig. 3. Strain mapping in the 2D configuration. (A) Schematic representation of the setup. (B) Displacement (d) as a function of the internal chamber pressure (p_i) calibration curve for gloss (G/G) silicone. (C) The series of images illustrating maximum displacement of the PDMS membrane at 10 psi and various nominal times (as indicated on the pictures). For the full list of nominal times and pressures refer to Table 2.

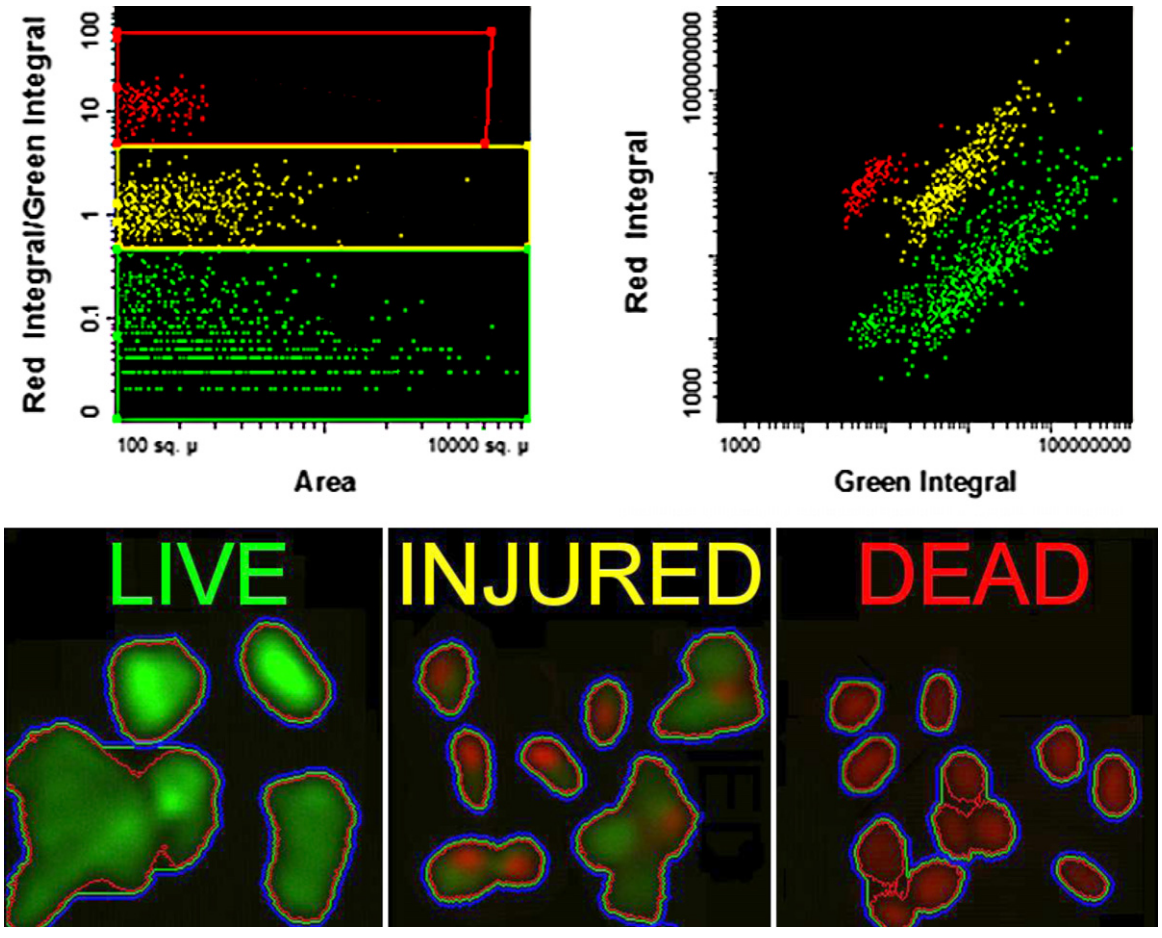

Fig. 4. The scattergrams of control sample used to verify validity of the ratiometric Live–Injured–Dead scale developed in this study (top panel). The dead, injured and live cells are marked with red, yellow and green color respectively (cell count was 1200 for presented sample). The representative fluorescent microscopy images of SH-SY5Y cells in these three categories are presented in the lower panel. The contouring patterns (blue, light green and red lines) are used to discriminate cells from background and integrate the signal intensity are depicted. (For interpretation of the references to color in this figure legend, the reader is referred to the web version of the article.)

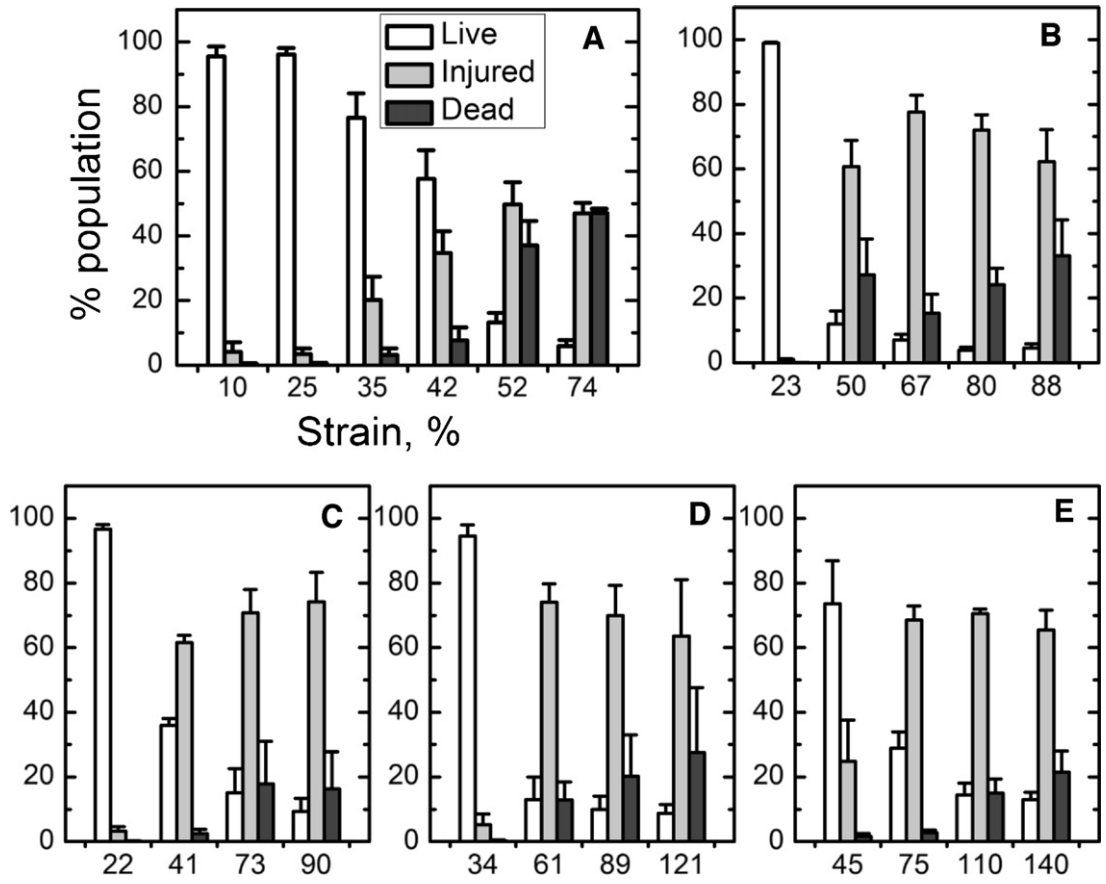

Fig. 5. The effect of the strain on the viability of SH-SY5Y cells subjected to different strain levels at different average strain rate, immediately post injury ($t = 0$): (A) 15 s^{-1}, (B) 25 s^{-1}, (C) 33 s^{-1}, (D) 42 s^{-1} and (E) 50 s^{-1}. Bars indicate average and error bars are SEM values. Each group tested at specific strain and strain rate consists of three populations of Live, Injured and Dead cells. For each tested group control sample was always present (Live >95%).

measurements formed the basis to define three categories of cells: (1) Live cells were characterized by the green/red (R/G) ratio below 0.5, (2) Injured cells were these with ratios in the range 0.5 < R/G < 5, and 3 Dead cells had R/G > 5 (Fig. 4). Later, we verified the method on a sample with all three categories of cells (Fig. 4, top panel).

2.6. Purification of polydimethylsiloxane (PDMS) substrate

During preliminary stage of the research, viability of non-treated control samples of cells seeded directly on PDMS was lower than expected. In these experiments population of live cells typically did not exceed 80–85% of the overall number of cells. The coating with PLLY mitigated this issue, to some extent, but the percentage of injured and dead cells was still relatively high (~10%). Preliminary results suggest leeching of non-crosslinked oligomeric silicone molecules is responsible for toxicity. We employed three-step purification protocol: (1) 24 h in D-PBS at 70 °C, (2) 24 h in ethyl acetate (99.9%, Sigma–Aldrich) at 75 °C, and (3) 24 h in deionized water at room temperature. PDMS purification resulted in high (live >95%) viability of the cells for all non-stretched controls.

2.7. Data analysis

Data are presented as mean ± standard error of the mean (SEM). One-way analysis of variance (ANOVA) is used to appraise the roles of strain magnitude and strain state. Unpaired two-tailed Student's *t*-tests were performed in order to assess statistical significance between samples, and *p*-values of <0.05 were considered significant.

3. Results

3.1. Strain history

Strain mapping measurements were performed using ARAMIS system equipped with high-speed Photron SA 1.1 cameras (Figs. 2 and 3). Pressure pulses with pre-defined nominal settings were collected for 23 points as listed in Table 2.

The strain gradient across the stretched membrane is a characteristic feature of this system (Fig. 2B), thus we used only center region where the strain field was relatively uniform (Geddes-Klein et al., 2006). To calculate biaxial strain of the silicone membrane, a simplified model derived by Winston et al. (1989) has been used (Morrison et al., 1998a):

$$\varepsilon_{\text{biaxial}} = \frac{2}{3}\left(\frac{w}{\alpha}\right)^2 - \frac{2}{15}\left(\frac{w}{\alpha}\right)^4 + \frac{2}{35}\left(\frac{w}{\alpha}\right)^6, \quad (1)$$

where a is the radius and w is the displacement of the center of circular membrane. In our case, strains measured by ARAMIS system fit this model very well (Fig. 2D, dashed line) in the broad range of displacements (0–12 mm). The deviation at higher displacements (>12 mm) indicates that the basic assumption that the edge boundary conditions are fixed is not valid. Thus, in order to cover the entire range, we developed purely empirical centerline displacement–maximum strain relationship (Fig. 2D) based on two sets of calibrations. In phase 1 image analysis yields a full strain map up to maximum strain value of approximately 100% because of software limitations (Fig. 2). In phase 2 (Fig. 3), we captured the membrane deformation history in the full range of displacements in the 2D setup. The two types of PDMS membranes used in these

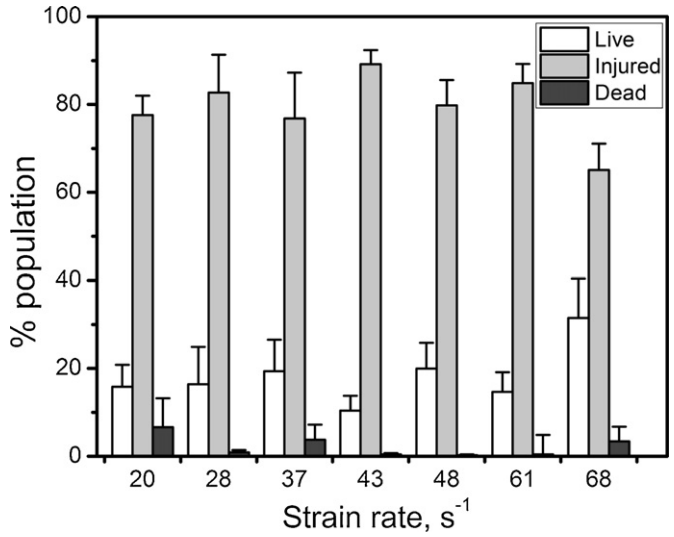

Fig. 6. The strain rate effect on the viability of SH-SY5Y cells subjected to stretch at fixed strain ($\varepsilon = 50\%$). These tests were performed immediately post injury ($t = 0$). There were no statistical differences between respective groups (Live and Injured cells) across tested strain rate range (*t*-test and one-way ANOVA).

tests (phase 1: M/M type and phase 2: G/G type) have the same elastic properties and thus the relationship between internal chamber pressure and displacement is almost identical (Figs. 2C and 3B, respectively). Hence, we can use one empirical function (Fig. 2D) to calculate strain values for all 23 nominal settings for G/G membrane type (Table 2), which was used in cell stretching studies. Similar approach was used in the past for non-uniform (Ellis et al., 1995) and uniform strain systems (Geddes and Cargill, 2001; Stroetz et al., 2001).

3.2. Ratiometric viability scale based on Live–Dead assay

The Live–Dead assay is a classical method to evaluate viability of cells and it has found widespread application on the neuroscience TBI research field (Cullen et al., 2007; LaPlaca et al., 2005; LaPlaca and Thibault, 1997). Calcein-AM (green), the acetomethoxy ester form of calcein, can penetrate the intact membrane of healthy cells. Intracellular esterases of viable cells cleave the ester group, which makes the calcein strongly fluorescent. Dead cells do not have functional esterases and cannot be labeled in this way. EthD-1 (red), a membrane impermeant fluorescent dye is used to stain dead cells exclusively. The viable cells with compromised membrane are stained green and red, and these cells are classified as injured (Fig. 4).

3.3. Strain and strain rate effect

The results of tensile testing performed at five discrete average strain rates (15–50 s^{-1}) and corresponding strains ranging from 0 to 140% are presented in Fig. 5 (total 23 combinations of strain and strain rates). Data analysis was performed on the central part of the deformed membrane with a radius of 4 mm which corresponds to 14% of the total area of the sample (see the circle in the inset of Fig. 1B). In this area according to recorded calibration data, the strain magnitude varied within ±5% of the calculated peak value. Samples where cell detachment was obvious were excluded from the analysis.

Sharp decrease in the number of viable cells with concomitant increment of injured and dead cells populations is noticeable with increasing substrate strain (Fig. 5). The effect of strain rate on viability is studied when the strain is fixed at a specific level. Fig. 6 shows the effect of $\dot{\varepsilon} = 20$ to 68 s^{-1} at a value of $\varepsilon = 50\%$. Despite the increase in strain rate, there are no statistical differences between tested samples ($p > 0.05$). These results suggest that with high strain level, strain rate is not an important factor during stretch injury.

3.4. Stretch-mediated dose response modeling

The injury profiles, *i.e.* data points for live and injured populations as a response to maximum substrate strain were fitted using dose–response function represented by Eq. (2):

$$y = A_1 + \frac{A_2 - A_1}{1 + 10^{(\log x_o - x)p}} \quad (2)$$

where $\log(x_o)$ – center of the curve, p – hill slope, and A_1, A_2 – bottom and top asymptote, respectively. These dose–response curves for $\varepsilon = 0$–100% are depicted in Fig. 7. Both plots present complementary data, *i.e.*, the population of injured cells increases sharply in the narrow strain range ($\varepsilon = 30$–55%) with corresponding decrease in live cell numbers. From these results, we identify three regions with different modes of injury: (I) mild, with predominantly live cells ($\varepsilon = 0$–30%), (II) moderate, where the transition between live and injured cells takes place ($\varepsilon = 30$–55%) and (III) severe with mainly injured and dead cells ($\varepsilon = 55\%$ and more).

3.5. Temporal injury evaluation

Since we are concerned with not only neuronal injury in the acute stages, but also progression post injury, we decided to pursue Live–Injured–Dead assay over 24 h period post-injury. The results of these tests performed at four discrete strain values ($\varepsilon = 42\%$, 50%, 73% and 90%) are presented in Fig. 8. Although cells suffered a significant injury after 42 and 50% stretch they gradually recuperated: 2 h post injury the recovery is almost complete (Fig. 8A and B). Cell injured at even higher stains ($\varepsilon = 73\%$ and 90%) just partially recovered in the analogous time period and viability deterioration is clearly visible within initial 24 h (Fig. 8C and D).

4. Discussion

The *in vitro* TBI models provide valuable insight into initial cellular trauma mechanisms and facilitate systematic evaluation of important biomechanical parameters such as strain and strain rate. In this study, we observed the effect of a wide range of strain of strain rate on SH-SY5Y cells. The control over strain in the device (Fig. 1) is achieved by adjusting values of nominal pressure and time (Table 2). In this way, the pressure pulses with precisely controlled duration and magnitude are generated. The high-speed imaging system allowed us to record membrane deformation in real time and precise calculation of strain and strain rates. Two sets of calibrations assured excellent repeatability (Fig. 2 and 3). Our primary research interest is to investigate *in vitro* the blast TBI (bTBI) effects, *i.e.* these characterized by low frequency (<0.5 kHz) high-amplitude shear waves that disrupt tissue by generating local motions and overcome natural tissue elasticity (Cernak and Noble-Haeusslein, 2010). However, the CAI device allows application of strain rates as high as 50 s^{-1}, *i.e.* at the lower end of the biomechanical loading conditions associated with blast exposure. Other research groups reported in the past maximum strain rates of 10 s^{-1} (Cargill and Thibault, 1996; LaPlaca et al., 1997), 1–10 s^{-1} (Geddes and Cargill, 2001), 15 s^{-1} (Morrison et al., 1998a) and 26–35 s^{-1} (Smith et al., 1999) for similar systems (2D cultures). Moreover, studies conducted by Bayly and co-workers concluded that TBI occurs at strain rates greater than 50 s^{-1} (Bayly et al., 2006). To achieve higher strain rates the internal volume of the sample chamber had to be decreased using toroidal silicone insert and evaluation of strain rates as high as 68 s^{-1} was thus possible.

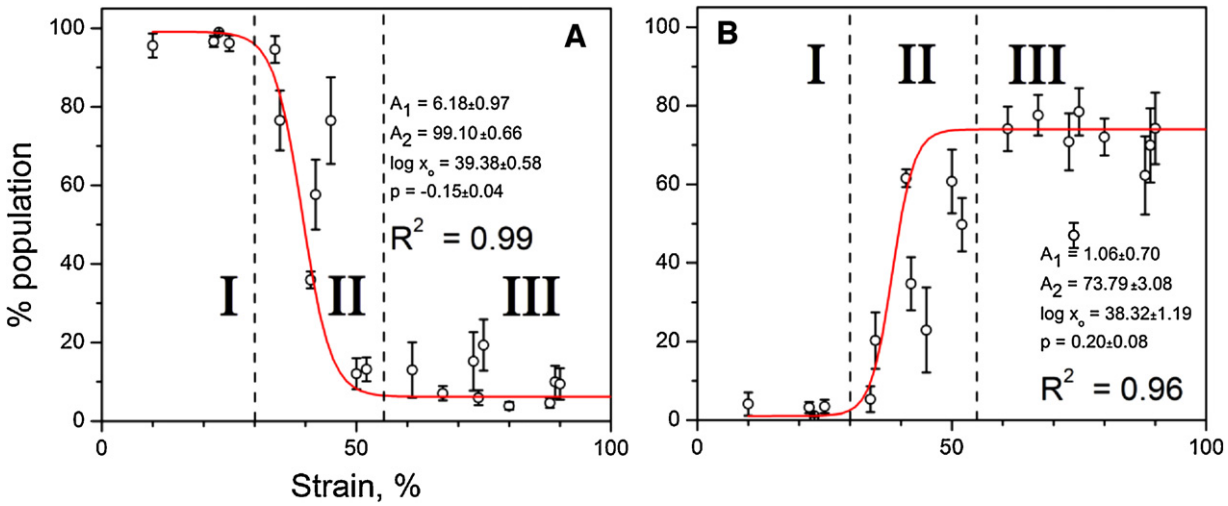

Fig. 7. The effect of the strain on the viability of SH-SY5Y cells subjected to different strain levels, immediately post injury ($t = 0$). The curves were constructed by pooling all the data together and subsequently, data points for populations of live (A) and injured (B) cells were fitted using Eq. (2). The decrease in population of live cells corresponds to concomitant increase in percentage of injured cells with increasing strain. The population of live cells is depleted in the range of 30–50% strain. Three injury regions are indicated in the plot A: I. mild: $\varepsilon = 0$–30%, II. moderate: $\varepsilon = 30$–55% and III. severe: $\varepsilon = 55\%$ and more.

Laser Scanning Cytometry is a well-suited technique for analysis of fluorescently labeled, glass slide mounted samples (Harnett, 2007); it offers excellent spatial resolution and signal quantification in cells and tissues, but surprisingly, it had not been used on neurotrauma research field. To the best of our knowledge, the approach presented in this paper (LSC and Live–Dead assay) is the first example of a fully automated, quantitative method for viability evaluation in TBI *in vitro* model. Analytical potential of LSC allowed us to define ratiometric Live–Injured–Dead scale (Fig. 4) and with this powerful tool, we evaluated a broad range of strain and strain rates (Fig. 5). Applied strain causes the gradual decrease of live cells fraction at the lowest strain rate tested ($\dot{\varepsilon} = 15\,s^{-1}$,

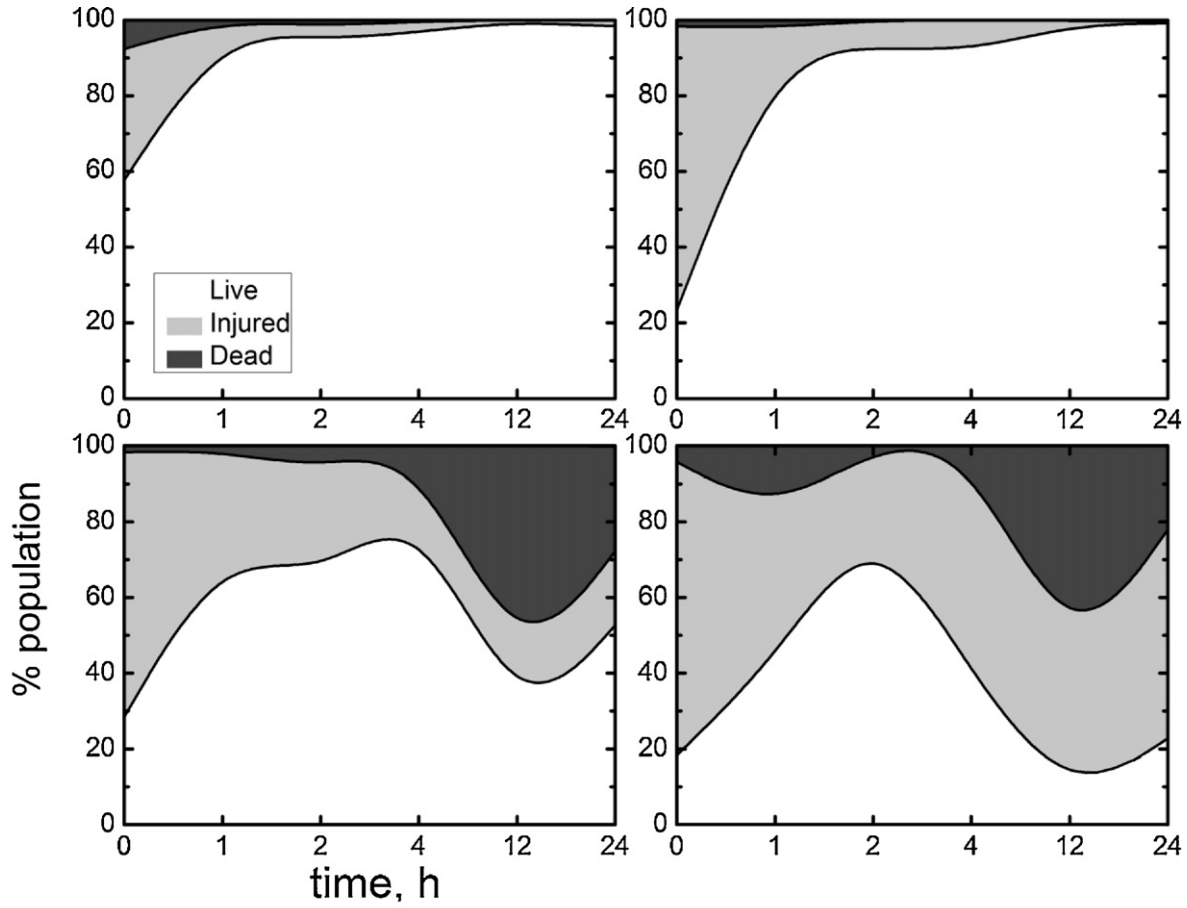

Fig. 8. Area plots of temporal injury development for cells exposed to strain magnitude of: (A) 42%, (B) 50%, (C) 73%, and (D) 90%. Samples were processed in triplicates (total 72 samples). Typically, SEM was lower than 5% for all time points.

Fig. 5A), but sharp decrease (below 40% of population) is clear for remaining samples when strain exceeds 40%. Correspondingly, injured cells are predominant for strains exceeding 40%. In the acute phase, the fraction of the dead cells remains rather low, reaching 30% at extreme strains ($\varepsilon > 90\%$), most probably due to instantaneous cell lysis. In the past similar analysis was performed with an aid of propidium iodide (PI), a cell membrane impermeant dye. Engel et al. (2005) observed increased PI uptake in primary mouse cortical neuron cultures immediately after the injury. The extent of injury scaled up with applied strain: at $\varepsilon = 30\%$ and 40% there were 30% and 40% of PI positive cells, respectively. In our case, at $\varepsilon = 30\%$ injured and dead cells constitute less than 10% of the population, but at $\varepsilon = 40\%$ the number of EthD-positive cells is similar (Fig. 7). The PI uptake decreased gradually after 24 and 48 h in these studies. It indicates cells with compromised plasmalemmal membrane are predominant, a result consistent with our observations in the respective strain range ($\varepsilon < 50\%$, Fig. 8B). Slemmer et al. (2002) reported 20%, 50% and 60% of PI positive cells on average at $\varepsilon = 30\%$, 40% and 72%, respectively. However, there were 10% PI stained cells in control samples. For astrocytes, the onset of injury was observed at strains as low as 31% (Ellis et al., 1995), in accordance with our results (Fig. 7). The numbers of injured and dead cells increased with applied strain (38–72%) and decreased with time post-injury (2, 6 and 24 h). Interestingly, these authors reported complete recovery of cells injured at $\varepsilon = 54\%$ after 48 h, a longer time than reported therein (Fig. 8B). It appears behavior of two neuronal cell lines in the acute phase immediately after the injury is similar to cells used in this contribution. Major differences are observed during the subacute recovery phase. It is possible these disparities stem from diverse defense mechanisms against plasma membrane disruption between different cell lines.

Cullen et al. (2007) reported strain rate dependent astrogliosis (increase in the number of astrocytes caused by destruction of adjacent neurons) in 3D neuronal-astrocytic co-cultures. These tests performed 2 days post-injury indicate the viability of samples exposed to 50% strain (shear model) decreased in the order of applied strain rates: 1, 10 and 30 s^{-1}, respectively. On the contrary, lack of cell viability-strain rate correlation was reported for organotypic hippocampal cultures exposed to 30 combinations of strain and strain rates ($\varepsilon = 5$–$50\%, \dot{\varepsilon} = 0.1 - 50\ s^{-1}$) (Cater et al., 2006). This indicates decreasing injury tolerance with increasing complexity of the strain field (2D < 3D) and points out to the strain level as a major injury factor. In our experiments, when the ε level was fixed at 50%, strain rate is not the decisive factor for the outcome (Fig. 6). Viscoelastic effects may not become pronounced when the strain effect is already dominant. We believe, however, this cannot be generalized to all other strain and strain rates, since at this strain level significant injury already occurred. Probably, at low strains and high strain rates there could be strain rate effect, which we plan to explore in the future.

Fig. 7 shows the viability of SH-SY5Y cells in the acute post-injury stage. While Fig. 7A shows the percentage change of live cells as a function of applied biaxial strain, Fig. 7B shows the percentage change of injured cells-both of these being measured in terms of fluorescence. Survival-applied strain shows a reversed S-shaped behavior, with two flat regions in the low (<30%) and high (>55%) strain levels with a very sharp variation from live to dead in region II (30–55%). In region II, the survival rate changes from 90% to almost 10% within a strain range of 25%, indicating that whatever mechanism becomes active, the injury leads to instantaneous death in a decisive manner. The error bands in region I or region III are rather narrow. Even at a very high magnitude of applied strain (*e.g.* 90%), the % viability has a very narrow range (within ±5%). The strain transferred from substrate to cell is a strong function of the material of the extracellular matrix (ECM), which regulates cell adhesion strength (Cargill et al., 1999). We have tested four proteins (collagen-I, fibronectin, laminin and PLLY) to select the most appropriate matrix for cell adhesion. It turned out only with application of PLLY, we observed statistically significant population of injured cells with respect to control at $\varepsilon = 50\%$ ($p < 0.05$, data not shown) and for this reason PLLY was used in all experiments. These observations indicate our injury model (culture + stretch + viability assay) is highly repeatable.

Non-specific membrane pores generated during stretch (the so called mechanoporation (LaPlaca et al., 1997; Pike et al., 2000; Simon et al., 2009)) allow an influx of membrane impermeable dye, EthD-1. This is seen as elevated numbers of injured cells in these area plots (Fig. 8). The radius of ethidium homodimer-1 molecule exceeds the size of calcium ion (Ca^{2+}: 0.114 nm, EthD-1: 0.836 nm (average value calculated using of equations 9 and 10 taken from Oliver et al., 1992)) and its presence in the cytosol is thus the evidence for mechanoporation and calcium influx (extracellular Ca^{2+} concentration is 1.8 mM in our experiments). Frequently, calcium cytosolic concentration ($[Ca^{2+}]_i$) increase is observed immediately after the neuronal injury (Cargill and Thibault, 1996; Geddes-Klein et al., 2006; Lusardi et al., 2004b). It was also demonstrated calcium transients in stretch-injured hippocampal neurons are proportional to the extent of injury expressed as strain magnitude and strain rate (Lusardi et al., 2004b). Hence, we expect the same mechanism is operating in our system, and elevated calcium concentrations will ultimately lead to the cell death. While exact mechanism at this point is not clear, it appears, however, propensity to follow necrotic rather than the apoptotic pathway depends on the intracellular Ca^{2+} concentration (Zipfel et al., 2000): elevated $[Ca^{2+}]_i$ and consequent necrosis are strongly related, and this mechanism can be used to explain a substantial increase of dead cells population after 12 h.

Geddes et al. (2003) used six probe molecules with molecular weights ranging from 380 Da (carboxyfluorescein) to 150 kDa (fluorescent conjugated dextrans) and sizes in the range 0.5–8.9 nm to study membrane permeability. These experiments concluded immediately after 30% stretch ($\dot{\varepsilon} = 10\ s^{-1}$) the molecular probes diffused into intracellular space, in just 5 min post-injury only the smallest molecule, carboxyfluorescein could penetrate the cell membrane. It is thus clear that the size of pores changes very quickly during short period of time post-injury and the time-dependent behavior is critical. Our data presented in Fig. 8 depict complementary set of experiments. We can clearly distinguish two phases: (1) acute, 1–4 h where primarily membrane repair takes place with very little evidence of cell death; (2) chronic, extending for more than 4 h post-injury. Moreover, it appears membrane re-sealing process depends on the magnitude of mechanical insult. However, while samples exposed to 43% and 50% strain recovered within 2 h and did not display any detrimental viability effects up to 24 h, the same cannot be said about samples injured at 73% and 90%. For these samples, there is a substantial population of injured cells after 2 and 4 h and the number of dead cells reaches maximum 12 h post-injury (Fig. 8C, D). Thus, based on dose–response curves and temporal injury profiles (Figs. 7 and 8) we can define the injury scale for SH-SY5Y cells: (I) mild: $\varepsilon = 0$–30%, (II) moderate: $\varepsilon = 30$–55%, and (III) severe: $\varepsilon > 55\%$.

In conclusion, in the extended *in vitro* TBI paradigm presented in this paper, we applied high-speed imaging system to precisely characterize PDMS membrane strain and strain rates. The model as built and calibrated allows the application of accurate and repeatable levels of strain and strain rate. The application of Laser Scanning Cytometry allows fully automated data acquisition and precise analysis of injury levels, with excellent spatial resolution. This technique helped us perform thorough analysis at various sets of experimental conditions. Dose–response analysis revealed there are 3 regions characterized by mild, moderate and severe injury levels, which was further corroborated by evaluation of temporal

insult profiles. We believe with our *in vitro* model will be useful in the precise evaluation of injury criterion and injury risk curves, that can then be used in a computational model. Such a model will ultimately aid in the understanding of TBI, and development of therapeutics.

Acknowledgements

Financial support under the US Army Research Office project "Army-UNL Center of Trauma Mechanics" (Contract No. W911NF-08-10483) is gratefully acknowledged. Partial financial support provided by the College of Engineering is acknowledged. We are grateful to Dr. Douglas Smith (University of Pennsylvania) for helpful comments during development of the injury model.

References

Arun P, Spadaro J, John J, Gharavi RB, Bentley TB, Nambiar MP. Studies on blast traumatic brain injury using in vitro model with shock tube. Neuroreport 2011;22:379–84.

Bayly PV, Black EE, Pedersen RC, Leister EP, Genin GM. In vivo imaging of rapid deformation and strain in an animal model of traumatic brain injury. J Biomech 2006;39:1086–95.

Bose A, Mouton-Liger F, Paquet C, Mazot P, Vigny M, Gray F, et al. Modulation of tau phosphorylation by the kinase PKR: implications in Alzheimer's disease. Brain Pathol 2011;21:189–200.

Cargill II RS, Thibault LE. Acute alterations in $[Ca^{2+}]_i$ in NG108-15 cells subjected to high strain rate deformation and chemical hypoxia: an in vitro model for neural trauma. J Neurotrauma 1996;13:395–407.

Cargill III RS, Dee KC, Malcolm S. An assessment of the strength of NG108-15 cell adhesion to chemically modified surfaces. Biomaterials 1999;20:2417–25.

Cater HL, Sundstrom LE, Morrison BI. Temporal development of hippocampal cell death is dependent on tissue strain but not strain rate. J Biomech 2006;39:2810–8.

Cernak I, Noble-Haeusslein LJ. Traumatic brain injury: an overview of pathobiology with emphasis on military populations. J Cereb Blood Flow Metab 2010;30:255–66.

Chen YC, Smith DH, Meaney DF. In vitro approaches for studying blast-induced traumatic brain injury. J Neurotrauma 2009;26:861–76.

Cullen DK, Simon CM, LaPlaca MC. Strain rate-dependent induction of reactive astrogliosis and cell death in three-dimensional neuronal-astrocytic co-cultures. Brain Res 2007;1158:103–15.

Decressac M, Pain S, Chabeauti PY, Frangeul L, Thiriet N, Herzog H, et al. Neuroprotection by neuropeptide Y in cell and animal models of Parkinson's disease. Neurobiol Aging 2011.

Elkin BS, Morrison BI. Region-specific tolerance criteria for the living brain. Stapp Car Crash J 2007;51:127–38.

Ellis EF, McKinney JS, Willoughby KA, Liang S, Povlishock JT. A new model for rapid stretch-induced injury of cells in culture: characterization of the model using astrocytes. J Neurotrauma 1995;12:325–39.

Engel DC, Slemmer JE, Vlug AS, Maas AI, Weber JT. Combined effects of mechanical and ischemic injury to cortical cells: secondary ischemia increases damage and decreases effects of neuroprotective agents. Neuropharmacology 2005;49:985–95.

Geddes-Klein DM, Schiffman KB, Meaney DF. Mechanisms and consequences of neuronal stretch injury in vitro differ with the model of trauma. J Neurotrauma 2006;23:193–204.

Geddes DM, Cargill II RS. An in vitro model of neural trauma: device characterization and calcium response to mechanical stretch. J Biomech Eng 2001;123:247–55.

Geddes DM, Cargill II RS, LaPlaca MC. Mechanical stretch to neurons results in a strain rate and magnitude-dependent increase in plasma membrane permeability. J Neurotrauma 2003;20:1039–49.

Harnett MM. Laser scanning cytometry: understanding the immune system in situ. Nat Rev Immunol 2007;7:897–904.

LaPlaca MC, Cullen DK, McLoughlin JJ, Cargill II RS. High rate shear strain of three-dimensional neural cell cultures: a new in vitro traumatic brain injury model. J Biomech 2005;38:1093–105.

LaPlaca MC, Lee VM, Thibault LE. An in vitro model of traumatic neuronal injury: loading rate-dependent changes in acute cytosolic calcium and lactate dehydrogenase release. J Neurotrauma 1997;14:355–68.

LaPlaca MC, Prado GR. Neural mechanobiology and neuronal vulnerability to traumatic loading. J Biomech 2010;43:71–8.

LaPlaca MC, Thibault LE. An in vitro traumatic injury model to examine the response of neurons to a hydrodynamically-induced deformation. Ann Biomed Eng 1997;25:665–77.

Lusardi TA, Rangan J, Sun D, Smith DH, Meaney DF. A device to study the initiation and propagation of calcium transients in cultured neurons after mechanical stretch. Ann Biomed Eng 2004a;32:1546–58.

Lusardi TA, Wolf JA, Putt ME, Smith DH, Meaney DF. Effect of acute calcium influx after mechanical stretch injury in vitro on the viability of hippocampal neurons. J Neurotrauma 2004b;21:61–72.

Morrison BI, Cater HL, Benham CD, Sundstrom LE. An in vitro model of traumatic brain injury utilising two-dimensional stretch of organotypic hippocampal slice cultures. J Neurosci Methods 2006;150:192–201.

Morrison BI, Elkin BS, Dolle JP, Yarmush ML. In vitro models of traumatic brain injury. Annu Rev Biomed Eng 2011;13:91–126.

Morrison BI, Meaney DF, Margulies SS, McIntosh TK. Dynamic mechanical stretch of organotypic brain slice cultures induces differential genomic expression: relationship to mechanical parameters. J Biomech Eng 2000;122:224–30.

Morrison BI, Meaney DF, McIntosh TK. Mechanical characterization of an in vitro device designed to quantitatively injure living brain tissue. Ann Biomed Eng 1998a;26:381–90.

Morrison BI, Saatman KE, Meaney DF, McIntosh TK. In vitro central nervous system models of mechanically induced trauma: a review. J Neurotrauma 1998b;15:911–28.

Nampiaparampil DE. Prevalence of chronic pain after traumatic brain injury: a systematic review. JAMA 2008;300:711–9.

Oliver III JD, Anderson S, Troy JL, Brenner BM, Deen WH. Determination of glomerular size-selectivity in the normal rat with Ficoll. J Am Soc Nephrol 1992;3:214–28.

Pfister BJ, Weihs TP, Betenbaugh M, Bao G. An in vitro uniaxial stretch model for axonal injury. Ann Biomed Eng 2003;31:589–98.

Pike BR, Zhao X, Newcomb JK, Glenn CC, Anderson DK, Hayes RL. Stretch injury causes calpain and caspase-3 activation and necrotic and apoptotic cell death in septo-hippocampal cell cultures. J Neurotrauma 2000;17:283–98.

Simon CM, Sharif S, Tan RP, LaPlaca MC. Spinal cord contusion causes acute plasma membrane damage. J Neurotrauma 2009;26:563–74.

Slemmer JE, Matser EJ, De Zeeuw CI, Weber JT. Repeated mild injury causes cumulative damage to hippocampal cells. Brain 2002;125:2699–709.

Slemmer JE, Weber JT, De Zeeuw CI. Cell death, glial protein alterations and elevated S-100 beta release in cerebellar cell cultures following mechanically induced trauma. Neurobiol Dis 2004;15:563–72.

Smith DH, Wolf JA, Lusardi TA, Lee VM, Meaney DF. High tolerance and delayed elastic response of cultured axons to dynamic stretch injury. J Neurosci 1999;19:4263–9.

Stroetz RW, Vlahakis NE, Walters BJ, Schroeder MA, Hubmayr RD. Validation of a new live cell strain system: characterization of plasma membrane stress failure. J Appl Physiol 2001;90:2361–70.

Winston FK, Macarak EJ, Gorfien SF, Thibault LE. A system to reproduce and quantify the biomechanical environment of the cell. J Appl Physiol 1989;67:397–405.

Zipfel GJ, Babcock DJ, Lee JM, Choi DW. Neuronal apoptosis after CNS injury: the roles of glutamate and calcium. J Neurotrauma 2000;17:857–69.